Earth and Space Science

RESEARCH ARTICLE
10.1029/2019EA000906

Key Points:
- The detected TCs using the CSIRO (resolution-dependent) scheme are a subset of the OWZP (resolution-independent) detections
- The CSIRO scheme performs better in the high-resolution model compared to the reanalysis that has underrepresentation of TC intensity
- The study observes comparatively better performance of the TC frequency characteristics using the resolution-independent tracking scheme (OWZP)

Supporting Information:
- Figure S1

Correspondence to:
P. H. Raavi,
praavi@student.unimelb.edu.au

Citation:
Raavi, P. H., & Walsh, K. J. E. (2020). Sensitivity of tropical cyclone formation to resolution-dependent and independent tracking schemes in high-resolution climate model simulations. *Earth and Space Science*, *7*, e2019EA000906. https://doi.org/10.1029/2019EA000906

Received 23 SEP 2019
Accepted 17 FEB 2020
Accepted article online 25 FEB 2020

Sensitivity of Tropical Cyclone Formation to Resolution-Dependent and Independent Tracking Schemes in High-Resolution Climate Model Simulations

Pavan Harika Raavi[1,2] **and K.J.E. Walsh**[1,2]

[1]School of Earth Sciences, University of Melbourne, Melbourne, Victoria, Australia, [2]ARC Centre of Excellence for Climate Extremes, University of Melbourne, Melbourne, Australia

Abstract In the present study, global tropical cyclone (TC) formation characteristics are estimated using two fundamentally different Commonwealth Scientific and Industrial Research Organisation (CSIRO) and Okubo-Weiss zeta parameter (OWZP) tracking schemes in the reanalysis data and in a high-resolution climate model with interannually varying sea surface temperatures. Both the schemes have a reasonable global geographical distribution of TC genesis locations with under simulation in the eastern North Atlantic and northwestern Australian regions. The mean annual TC frequency in the model is similar to observations using the CSIRO scheme but higher using the OWZP scheme, whereas the annual frequency in reanalysis using the OWZP scheme is similar to observations but halved using the CSIRO scheme. In the CSIRO scheme, both the resolution-dependent thresholds and large-scale climate may play a role for skilful TC formation statistics. In contrast, large-scale climate leads to changes in OWZP TC detections. This highlights the importance of the large-scale environment for TC detections in both the tracking schemes. The OWZP scheme can differentiate the monsoon lows from the actual TCs in the north Indian Ocean compared to the CSIRO scheme, which incorrectly detects them as TCs in the monsoon season. The distribution of TC lifetime in the model using the OWZP scheme is similar to observations. Conversely, the CSIRO scheme detected TCs have shorter lifetimes, perhaps due to intrinsic tracking scheme differences. Although the tracking schemes are fundamentally different, the study shows that there exist some similarities between them and for certain TC formation characteristics the OWZP scheme performs better compared to the CSIRO scheme.

Plain Language Summary As the climate models act as the best tool to understand the relationship between the climate and TC formation, the TC research world is moving toward the high-resolution climate models with improved parameterization schemes to understand TC formation characteristics in the current climate better and improve the confidence in future projections. In the current study, a high-resolution atmospheric climate model is used to observe the performance of two different tracking schemes when compared with observations in simulating different TC characteristics like geographical distributions, mean annual numbers, the influence of El Niño (La Niña), and interannual and seasonal variability of TC frequency. Of the two schemes employed, one scheme is the traditional CSIRO tracking scheme that detects TC-like vorticities and the other scheme, using the Okubo-Weiss zeta parameter, a phenomena based scheme, detects the circulations that have the potential for TC formation. The Okubo-Weiss zeta parameter scheme has superior performance in simulating the TC frequency characteristics compared to the CSIRO scheme.

1. Introduction

Recent advances in climate models have led to more accurate simulation of the tropical cyclone (TC) climatology, geographical distribution, and seasonal and interannual variability across various regions of the globe (Bell et al., 2013; Camargo & Wing, 2016; Li & Sriver, 2018; Shaevitz et al., 2014; Strachan et al., 2013; Tory et al., 2013b; Walsh et al., 2015; Zhao et al., 2009). The fine-resolution climate model simulations are particularly crucial for individual ocean basins where the low-resolution models have low skill in simulating TC formation rates comparable to observations. This results in higher variability between models in

individual basins, which leads to lower confidence in their future projections (Knutson et al., 2010). A study by Walsh et al. (2013) showed that a specific relationship exists between model resolution and TC formation rate even after applying resolution-based thresholds. Also, they demonstrated that high-resolution models had better TC formation patterns and rates.

Various observational and modeling studies have investigated the relationship between climate and TC formation. It is observed that different climate models produce distinct frequency rates across different ocean basins, and the precise cause for these variations is not clear. However, these earlier studies identified some of the prominent factors that lead to changes in TC formation rates. These factors include temporal and geographical variations of sea surface temperature (SST) (Gray, 1968; Murakami, Mizuta, & Shindo, 2012; Vecchi & Soden, 2007); midtroposphere relative humidity (Bister & Emanuel, 1997; Tang & Emanuel, 2010), vertical wind shear (VWS), McBride & Zehr, 1981; Riemer et al., 2010; Davis & Ahijevych, 2012), and a preexisting convective environment (Hendricks et al., 2004). In addition to the above variables, other factors that lead to changes in TC formation rates are the model convective parameterization schemes (Kim et al., 2012; Zhao et al., 2012) and also different TC tracking schemes with discrete choice of thresholds, storm duration, and formation latitudes (Camargo et al., 2005; Walsh et al., 2007; Horn et.al., 2014).

Using analysis from observations, TC formation research has been aided by the recent "marsupial pouch" concept defined within easterly waves of the Atlantic and Pacific regions (Dunkerton et al., 2009; Montgomery et al., 2012). This TC formation theory observes that TC formation occurs in semi-enclosed circulation regions (pouches) of easterly waves protected from surrounding influences like the entry of lower entropy drier air and high VWS. The protective pouch concept was later developed to identify the regions of TC formation potential (Wang et al., 2009; Wang et al., 2010a, b; Wang, 2012; Montgomery et al., 2010). Based on the pouch concept, in recent studies by Tory et al. (2013a), Tory et al. (2013b), a TC tracking scheme is developed using ERA-Interim reanalysis (Dee et al., 2011) that includes a diagnostic term known as the Okubo-Weiss Zeta parameter (OWZP), coexisting with necessary thermodynamic conditions and dynamic conditions. This OWZP represents low-deformation vorticity regions favorable for TC formation. The detected pouch locations in reanalysis using this tracking scheme have a close resemblance to observed TC genesis locations (International Best Track Archive for Climate Stewardship [IBTrACS]; Knapp et al., 2010) with 95% of the global TCs containing enhanced values of OWZ, not limited to the regions of tropical easterly waves in the Atlantic and Pacific regions. Bell et al. (2018) statistically assessed TC track climatology in ERA-Interim reanalysis using the OWZP scheme and noted good agreement between observed and detected tracks. In addition, this scheme is resolution independent and also observed to have consistent results of TC frequency as well as track changes both in current and future climate using various Coupled Model Intercomparison Project Phase 5 (CMIP5) models (Tory, Chand, McBride, et al., 2013; Bell, Chand, Tory, Dowdy, et al., 2019; Bell, Chand, Tory, Turville, et al., 2019).

It would thus be useful to apply these concepts to the output of fine-resolution climate models, as a way of better defining and detecting TCs in model output. Existing TC tracking schemes tend to be resolution dependent and use wind speed or vorticity thresholds (Horn et al., 2014; Shaevitz et al., 2014). Studies using climate models are moving to a higher horizontal resolution to better simulate and understand TC characteristics. It has been suggested that horizontal resolutions in the range of 20–100 km may be sufficient to study many aspects of the genesis and storm distribution (Oouchi et al., 2006; Bengtsson, Hodges, & Esch, 2007; Bengtsson, Hodges, Esch, Keenlyside, et al., 2007). In the present study, a high horizontal resolution model of about 40 km, the atmosphere-only Australian Community Climate and Earth-System Simulator (ACCESS) model (Bi et al., 2013), is used to detect present-day TCs using two different tracking schemes across different ocean basins, with basin boundaries given in Table S1 of the supporting information section. The first scheme is the circulation-based OWZP tracking scheme of Tory, Dare, Davidson, et al. (2013), and the second method is the Commonwealth Scientific and Industrial Research Organisation (CSIRO) detection scheme of Horn et al. (2014), a traditional TC tracking scheme that uses imposed thresholds such as minimum low-level wind speed. The OWZP detection scheme has not been examined for its performance in high-resolution models, whereas the CSIRO scheme has. Therefore, this study compares the performance of the phenomenon-based tracking scheme (OWZP) with the traditional scheme (CSIRO) in a fine-resolution climate model simulation and reanalysis when compared against the observations

(IBTrACS, Knapp et al., 2010) in simulating various storm characteristics such as climatology, lifetime, and seasonal and interannual variability. A particularly challenging region of the globe for TC tracking schemes is the North Indian (NI) Ocean basin, due to the prevalence of monsoon depressions in this basin that can be misidentified as TCs. Accordingly, some of the tracking schemes apply additional thresholds to remove the monsoon depressions falsely detected as TCs to capture the seasonal cycle correctly across this basin (Murakami, Mizuta, & Shindo, 2012). Therefore, we also attempted to examine the performance of the OWZP TC detection scheme in the NI Ocean.

2. Model, Data, and Methods

2.1. ACCESS Atmospheric Model and Simulation

In the current study, we employ the atmospheric component of the ACCESS general circulation model (GCM) (ACCESS 1.3, Bi et al., 2013). The description of this modeling system mostly follows that contained in the previous work using a similar model (Sharmila et al., 2020). This ACCESS model uses the atmospheric part of the UK Met Office Unified Model (UM v8.5) with improved parameterization schemes of the Global Atmosphere (GA 6.0) configuration. It includes the Joint UK Land Environment Simulator land surface model (Best et al., 2011; Walters et al., 2017). The dynamical core of the atmosphere within the model uses the semi-implicit semi-Lagrangian approach in a longitude-latitude grid, solving both the large-scale processes (solar and terrestrial radiation, precipitation, and gravity wave drag) and subgrid-scale processes (boundary layer processes, convection, atmospheric aerosols, and chemistry). A prognostic cloud fraction and prognostic condensate (PC2) scheme are employed (Wilson et al., 2008). The model also uses the radiation scheme of Edwards and Slingo (1996) for representing the cloud droplets, the boundary layer scheme of Lock et al. (2000) with additional modifications for representing the boundary layer, as described in Lock (2001) and Brown et al. (2008).

The model is run in an atmospheric mode with prescribed monthly and interannually varying Atmospheric Model Intercomparison Project SSTs (Kanamitsu et al., 2002) as a lower boundary condition and has a 40 km horizontal resolution with 17 vertical levels. The model is initialized with the atmospheric conditions of 1 September 1988 and integrated till 31 December 2010, using the Atmospheric Model Intercomparison Project SSTs and seasonally varying radiative forcing. Sharmila et al. (2020) evaluated the performance of this model in simulating large-scale climate variables in comparison to the observed climate variables of ERA-Interim reanalysis. They noted certain regional biases in large-scale fields of the model corresponding well with the genesis biases using the CSIRO scheme. Keeping in view the model performance, we compare the model and reanalysis performance in simulating the TC formation characteristics with IBTrACS for 20 years from 1990 to 2009 using two fundamentally different tracking schemes.

2.2. Observational and ERA-Interim Data

In the current study, we use the IBTrACS TC data for the 1990–2009 period. This comprises information from the different regional TC observing centers synthesized and merged together into a single data set (Knapp et al., 2010). For the years analyzed here, the IBTrACS data should have an almost complete representation of TC formation, although Knapp et al. (2010) note small differences between the operational centers that compile the best track data in the total number of declared TCs (see also Hodges & Emerton, 2015; Ren et al., 2011). Here IBTrACS serves as ground truth for TC formation. An issue in all best track data sets is the lack of a consistent definition of extratropical transition between operational centers, which leads to biases in the length of the observed TC tracks (Schreck et al., 2014).

The TCs simulated in the reanalysis data act as a bridge between the TCs simulated in a GCM and the observed TCs. The reanalysis data are spatially and temporally homogeneous assimilated observation data but have some constraints. These include the resolution of the model used to produce the reanalysis, the model physics, and the type of assimilation methods. Nevertheless, compared to the earlier reanalysis versions, the ERA-Interim has improved model physics and includes the use of four-dimensional variational data assimilation (Compo et al., 2011; Dee et al., 2011). Recent studies showed that TC intensity is underestimated in the ERA-Interim reanalysis compared to the observations (Hodges et al., 2017; Murakami, 2014).

Two different TC tracking schemes are applied to the ERA-Interim data at a resolution of 0.75 ° × 0.75° at 12-hourly intervals for 20 years from 1990 to 2009. The OWZP tracking scheme requires the zonal and meridional wind fields at 850, 500, and 200 hPa pressure levels to estimate the OWZ, the magnitude of vector wind difference between 200 and 850 hPa (the VWS), and the TC steering velocity (average wind at 700 hPa within a box region). In addition to the above variables, it requires relative humidity at 950 and 700 hPa levels, and specific humidity at the 950 hPa level. Similarly, the CSIRO tracking scheme requires the 10 m, 850 hPa, and 300 hPa zonal and meridional winds and mean sea level pressure.

2.3. OWZP TC Detection and Tracking Scheme

The OWZP tracking scheme (Tory, Dare, Davidson, et al., 2013; Tory et al., 2013a) detects the circulation regions within the "marsupial pouch" using a diagnostic quantity, a product of a normalized Okubo-Weiss parameter, and absolute vorticity (the OWZ parameter) along with certain thermodynamical and dynamical conditions. The OWZ parameter detects the low-deformation vorticity regions within the large-scale disturbances that have the potential for TC formation. The OWZ parameter is defined as follows:

$$\mathrm{OWZ} = \max(\mathrm{OW}_{\mathrm{norm}}, 0) \times (\zeta + f) \times \mathrm{sign}(f) \tag{1}$$

Here $\mathrm{OW}_{\mathrm{norm}}$ is the normalized Okubo-Weiss parameter, ζ is the relative vorticity, f is the planetary vorticity, $\zeta + f$ is the absolute vorticity, while E and F represent the stretching and shearing deformation, respectively:

$$\mathrm{OW}_{\mathrm{norm}} = \frac{\zeta^2 - (E^2 + F^2)}{\zeta^2};\ \zeta = \left[\frac{\partial v}{\partial x}\right] - \left[\frac{\partial u}{\partial y}\right]; E = \left[\frac{\partial u}{\partial x}\right] - \left[\frac{\partial v}{\partial y}\right];\ F = \left[\frac{\partial v}{\partial x}\right] + \left[\frac{\partial u}{\partial y}\right] \tag{2}$$

The detection scheme involves a sequence of steps from the initial detection to the final declaration of the circulation track as a TC (Tory, Dare, Davidson, et al., 2013; Tory et al., 2013a). The steps involved are as follows.

(i) In the first step, the algorithm identifies the grid points that satisfy certain initial thresholds of OWZ (low-deformation vorticity regions) at the 850 and 500 hPa pressure levels, as well as relative humidity thresholds at 950 and 700 hPa pressure levels, specific humidity at 950 hPa, and VWS, as shown in Table S2. The nearby grid points satisfying these conditions are combined into a clump that represents the storm position at the selected point of time.

(ii) In the second step, these clumps are tracked forward in time, and each clump position along the track is verified against certain additional core threshold conditions given in Table S2. The clumps that satisfy these conditions are declared as "True" otherwise "False." A track is terminated when there is no detected circulation forward in time by using a search algorithm that considers the forward circulation position estimated from the 700 hPa steering wind.

(iii) In the third step, the tracks constructed in step (ii) are further checked to see which track is to be considered as a TC. A track is declared as a TC if it satisfies the core thresholds for 48 h, having five consecutive "True" clumps in data with an archive interval of 12 h. The fifth consecutive True location along the track is considered as the TC genesis location (Bell et al., 2018).

2.4. CSIRO TC Detection and Tracking Scheme

The current study uses the modified CSIRO scheme, which is a traditional TC tracking algorithm that detects TC-like vortices using certain resolution-dependent objective thresholds. The following description follows that of Horn et al. (2014). The thresholds to be satisfied to declare a low-pressure system as a TC are the following:

(i) an absolute value of 850 hPa cyclonic vorticity should be higher than $1 \times 10^{-5}\ \mathrm{s}^{-1}$ to avoid grid points having weaker vorticity;

(ii) a closed pressure minimum with a 350 km distance in both x and y directions from the location satisfying the first condition is taken as the center of the storm;

(iii) mean wind speed within a 700 km × 700 km box region around the center of the storm at 850 hPa pressure level is to be higher than wind speed at the 300 hPa;

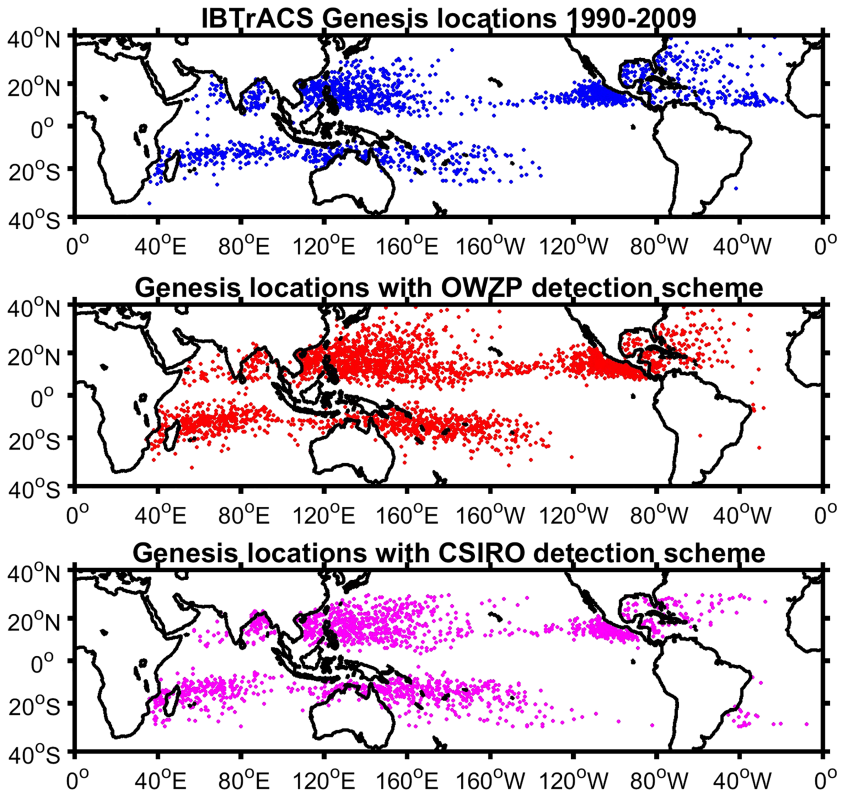

Figure 1. TC genesis locations in observations and the ACCESS model (using both CSIRO and OWZP schemes) for a period of 20 years from 1990 to 2009.

(iv) the maximum 10-m wind speed should exceed the resolution-dependent value, as proposed by Walsh et al. (2007). The wind speed threshold is 16.5 m/s for the 40 km horizontal resolution ACCESS model data and 15.5 m/s for the lower-resolution ERA-Interim reanalysis; and
(v) finally, the above conditions are to be satisfied for 24 consecutive hours for them to be declared as a TC.

3. Results and Discussion

3.1. Simulated TC Formation Characteristics

The quality of the TC formation climatology in the current climate is essential for any climate model to obtain reliable TC projections under changing climate conditions.

3.1.1. Geographical Distribution of TC Genesis Locations

This section illustrates the geographical distribution of the TC genesis locations from IBTrACS and the ACCESS model detected using both CSIRO and OWZP TC tracking schemes (Figure 1). The OWZP detected TCs are more frequent than observations in most of the ocean basins with an undersimulation in the eastern NA and northwestern part of the Australian (AUS) region. In contrast, the CSIRO detection scheme has larger undersimulation in the NA basin. From this, we notice that the ACCESS model simulates reasonably well the TC climatology, and both the tracking schemes identify the TC genesis detections at geographically similar locations to the observations. Similarly, the genesis locations in the reanalysis (Figure S1) have a close resemblance to observations using both the schemes.

Figure 2 shows the zonal and meridional distribution of TC genesis locations expressed in terms of a mean frequency at each 4-degree grid box across the globe. The zonal mean distribution has two peaks, one in the Northern Hemisphere (NH) and the other in the Southern Hemisphere (SH) at around 15° latitude in the observations (IBTrACS). There is a good agreement in the zonal distribution between the detected TCs of the model and reanalysis using both the schemes and observations (IBTrACS). Both the schemes have peak locations at similar latitudes except with a few more detections in the model at these latitudes using the

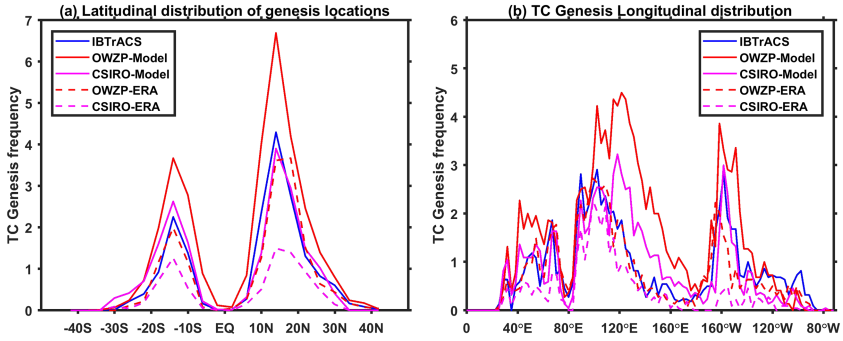

Figure 2. Zonal (a) and meridional (b) mean TC frequency (per 4°×4° box region across the globe) as a function of latitude and longitude in both observations and model (using both the CSIRO and OWZP detection schemes).

CSIRO scheme in the SH and significantly more detections using the OWZP scheme in both hemispheres. Similarly, from the meridional distribution of mean TC genesis frequency in IBTrACS, Figure 2 shows two sharp peaks, one at around 90°E in the South Indian (SI) Ocean and the other at 110°W in the eastern North Pacific (ENP) region. Also, there is a broader peak at around 150°E in the western North Pacific (WNP) and South Pacific (SP) regions. The meridional distribution in the reanalysis is similar to the observations using both the schemes. The CSIRO detections within the model have peaks at similar longitudes but with an eastward shift of the 150°E peak. In contrast, the OWZP detection scheme in the model has a 150°E (WNP and SP) peak shifted further eastward. There exists a peak at around 85°W and 70°W (ENP and NA) in the model using the OWZP scheme, which is not present using the CSIRO scheme. Therefore, the zonal and meridional mean TC frequency distributions in the model show differences across the ENP, NA, SP, and WNP basins for both the schemes when compared against observations.

3.1.2. TC Genesis Density Bias

Here the global TC genesis density is defined as the number of storms per year and per 4°×4° box region across the globe, as shown in Figures S2 and S3 for both model and ERA-Interim data, respectively. To understand the quantitative differences between the detection schemes in simulating TCs, we calculate the genesis density bias by subtracting the observations (IBTrACS) from the model and reanalysis detected TCs, and Table S3 and Table S4 show its basin-averaged values. These basin-averaged values in the reanalysis show that the CSIRO scheme has a negative bias in almost all the ocean basins compared to the OWZP scheme, which performs better in most of the ocean basins. In the model, basin-averaged values show a negative genesis bias in the NA-MDR with both the schemes and in the ENP basin using the CSIRO scheme.

The spatial genesis density bias (Figure 3) has similarities between both the tracking schemes in the model in the NI, SI, SP, and the AUS basins with a similar sign of the bias in the two schemes but with different magnitudes. There exist two basins with significant differences between both the schemes in the model: one being the NA-MDR basin, having negative bias using both the schemes with significantly higher negative bias using the CSIRO scheme (Table S3). The OWZP scheme is able to capture the NA-MDR genesis frequency within the model to some extent that is difficult to capture in most climate models (Walsh et al., 2016). The other basin showing substantial differences between the schemes is the ENP with strong positive bias throughout the basin using the OWZP detection, while the CSIRO scheme shows overall negative bias across the basin. In addition, the WNP basin within the model has patches of negative bias using the CSIRO scheme. From these differences, we can infer that the OWZP scheme has better performance in the NA-MDR, WNP, and ENP basins within the model compared to the CSIRO scheme, which has negative genesis density bias in these regions. To understand genesis biases (positive/negative) across the ocean basins, we perform a climatological analysis of climate variables.

Previously performed basinwise analysis of this model noted a relationship between TC genesis locations detected using the CSIRO scheme and the large-scale climate of the model (Sharmila et al., 2020). Following the analysis of Sharmila and Walsh (2017), the current analysis includes both dynamical variables such as omega at 500 hPa, VWS between 850 and 200 hPa, and 850 hPa relative vorticity ($Rvor_{850}$), along with thermodynamic variables including the maximum potential intensity (MPI) and the 700 hPa relative

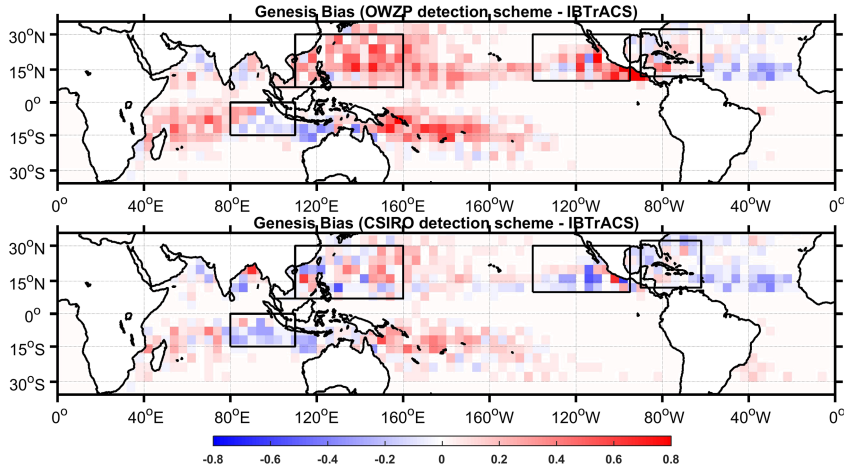

Figure 3. TC genesis density bias in the model using the CSIRO and OWZP tracking schemes when compared against observations (IBTrACS). TC genesis density is defined as the number of storms per 4° ×4° box region across the globe for a 20 year period from 1990 to 2009. The black rectangular boxes indicate the major differences in genesis density between the two schemes when compared with observations.

humidity (RH_{700}). The climatological analysis of the large-scale atmospheric fields for TC peak seasons (July, August, September (JAS) for NH; October, November, December over NI; January, February, March for SH) in both the ACCESS model and ERA-Interim reanalysis reveals some of the possible causes behind the TC genesis bias. From this analysis, we notice that higher values of VWS and midlevel omega (implying descent), lower values of RH_{700}, MPI, and $Rvor_{850}$ lead to negative genesis density bias using both the schemes across different ocean basins (not shown). Conversely, higher values of RH_{700}, MPI, and $Rvor_{850}$ and lower values of midlevel omega lead to positive bias with both the schemes. The more positive TC genesis density bias in the model using the OWZP detection compared to observations may be due to the more favorable large-scale climate within the model. Therefore, both the schemes show a relationship between genesis bias and the large-scale environment of the model.

3.1.3. Mean Annual Number of TCs

Every year around 80 cyclones form across the globe under certain dynamical and thermodynamical conditions (Emanuel, 2003; Gray, 1975). The asymmetry of global annual mean TC formations in the NH and the SH is comparable to the observations using both the schemes (Figure S4). In addition, the SH is found to be more active in the model compared to observations. Figure 4a summarizes the basin-wide mean annual frequency of the observed TC genesis along with the model-simulated TCs using both the detection schemes over the 20 year period. The global annual mean TC detections identified in the model output with the OWZP scheme is 143, whereas IBTrACS observations have 82.4 detections. The OWZP detection scheme shows 50% more TCs than the observed annual TC numbers, a statistically significant difference. In contrast, the mean annual TC number in the model with the CSIRO detection scheme is 86.

We have performed a similar analysis with ERA-Interim data, also for 20 years from 1990 to 2009. The mean annual number of detections using the OWZP scheme in the ERA-Interim is 75, which is close to the observations. In contrast, with the CSIRO detection scheme, the mean annual TC frequency is 36.5, which is 50% less than observations, as shown in Figure S4. The finer resolution in the ACCESS model data (0.36°) compared to the reanalysis (0.75°) leads to an increased number of detections in the model with both the tracking schemes. The increased TC detections with increasing resolution using the CSIRO detection scheme may be due to a more favorable large-scale climate and better simulation of TC intensity in high-resolution models. The resolution-dependent 10 m wind speed threshold is derived from the azimuthal mean TC intensity profile (Walsh et al., 2007). Murakami (2014) also noted that the CSIRO detection scheme underestimates annual TC numbers in low-resolution reanalysis indicating that the TC intensity is too weak in reanalysis data sets for its resolution if the only effect of the resolution is horizontal smoothing. In contrast, the more favorable large-scale climate within the model leads to more detections using the OWZP scheme compared to the reanalysis.

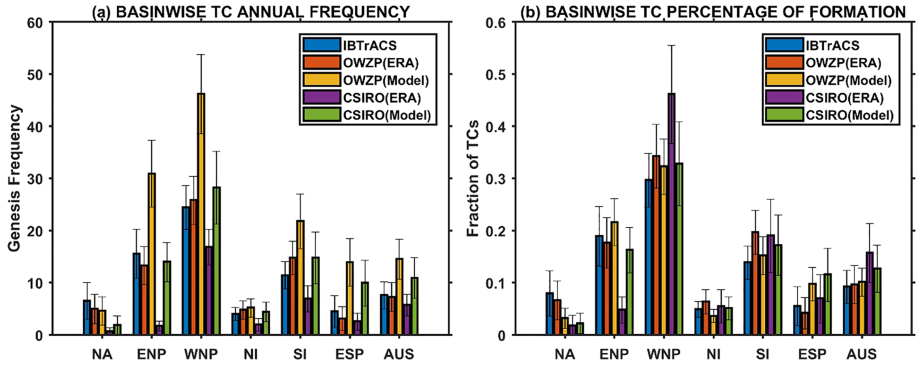

Figure 4. Basinwise mean annual number of TC genesis detections in the ACCESS model and ERA-Interim using both CSIRO and OWZP detection schemes and IBTrACS. (a) The total number of TCs and (b) the fraction of TCs in each basin compared to the global number of TCs.

Figure 4b shows the relative percentage of the storms detected by both the tracking schemes in the model and reanalysis across each of the ocean basins; for instance, the highest number of detections in the WNP basin is reproduced similar to the IBTrACS. The fraction of TCs in reanalysis using the CSIRO scheme shows that they have more TCs in the WNP and very few TCs in the NA. Therefore, the resolution-independent scheme (OWZP) is observed to have superior performance in simulating TC mean annual numbers and fraction of TCs in both the ACCESS model and ERA-Interim reanalysis data compared to the resolution-dependent CSIRO scheme.

3.1.4. Seasonal Cycle of TC Genesis Frequency

The seasonal cycle of TC formation across different ocean basins using both CSIRO and OWZP detection schemes with ACCESS model output is compared with IBTrACS, as shown in Figure S5. It is observed that both the model and reanalysis data can capture the seasonal cycle in all the ocean basins except in the NI Ocean, with good similarity to observations using both the schemes with the statistical correlations given in Table 1. The seasonal cycle in the NI Ocean has a bimodal distribution with two observed peaks in the premonsoon and postmonsoon seasons (observations) and is not captured well with CSIRO detection scheme in both the model and reanalysis but captured reasonably well using the OWZP detection scheme. The NI basin is where GCMs with some tracking schemes have difficulty in capturing the seasonal signal due to false alarms of monsoon depressions being identified as TCs during the monsoon season (Murakami, Mizuta, & Shindo, 2012; Murakami et al., 2013; Manganello et al., 2012; Camargo et al., 2016). The reason could be that monsoon depressions have certain similar characteristics with actual TCs (Murakami et al., 2011). The CSIRO detection scheme has higher TC detections in the monsoon season (July and August) in the ACCESS model, which degrades the simulated seasonal cycle across this basin.

Table 1
Basinwise Seasonal TC Frequency Correlations Between IBTrACS Observations and the Two Detection Schemes Applied to ACCESS Model Output

Basin	OWZP (model)	CSIRO (model)	OWZP (ERA)	CSIRO (ERA)
MDR_NA	**0.92***	**0.71***	**0.97***	**0.94***
ENP	**0.97***	**0.99***	**0.99***	**0.85***
WNP	**0.99***	**0.97***	**0.99***	**0.99***
NI	**0.67***	0.24	**0.86***	0.27
SI	**0.96***	**0.95***	**0.88***	**0.97***
SP	**0.94***	**0.98***	**0.89***	**0.95***
AUS	**0.96***	**0.97***	**0.88***	**0.97***

Note. Bold letters indicate statistically significant values;
*Indicates above 95% significance level.

3.2. Interannual Variability

The most dominant natural mode of climate variability in almost all the ocean basins, the El Niño and Southern Oscillation (ENSO) phenomenon, is observed to influence the interannual variability of TC genesis frequency and its characteristics (Bell et al., 2013; Camargo et al., 2010). Therefore, in the current section, we have investigated the model's performance in simulating the basin-wide interannual variability of the mean annual TC frequency in the ACCESS model using both the detection schemes when compared with the observed annual frequency. Table 2 shows the interannual correlations between IBTrACS and detected annual TCs using both the detection schemes applied both to the model output and to reanalysis. Overall, the detection schemes give better correlations when applied to reanalysis than to the model output. More so, the OWZP scheme appears to give better correlations than the CSIRO scheme, particularly in the reanalysis. We note that the correlations in Table 2 are from a single simulation. The interannual correlations of TC

Table 2
Correlations of the Interannual Variability of Annual TC Genesis Detections From the Model Using Two Different Tracking Schemes Compared With IBTrACS Observations

Basin	OWZP (model)	CSIRO (model)	OWZP (ERA)	CSIRO (ERA)
MDR_NA	**0.59***	**0.52***	**0.88***	**0.68***
ENP	0.3	**0.62***	**0.79***	0.2
WNP	**0.58***	0.22	**0.7***	**0.53***
NI	−0.12	0.18	0.38	0.03
SI	0.06	0.26	**0.51***	0.29
SP	0.07	0.14	**0.8***	**0.63***
ESP	0.24	0.15	**0.79***	**0.73***
AUS	**0.48***	−0.09	**0.55***	0.12

Note. Bold letters indicate statistically significant values; *indicates 95% significance level.

annual count with observations in atmospheric GCMs tend to improve in ensemble model simulations (Shaevitz et al., 2014; Strachan et al., 2013; Vitart et al., 1997; Vitart et al., 1999).

We further examine the model's ability to capture the variations in TC genesis locations during different phases of ENSO due to changes in atmospheric circulation patterns for a period of 20 years from 1990 to 2009. The model is run with interannually varying SSTs, and this partially transmits the observed ENSO signal; therefore, the NH (SH) El Niño and La Niña years within the model are considered similar to observations. The composites of TC genesis frequency per 4-degree box region across the global ocean basins are computed for El Niño and La Niña years given in Table S5 separately for the NH and SH (Sharmila et al., 2020). We use the definition of the ENSO index (the Oceanic Niño Index from the Climate Prediction Centre of the National Oceanic and Atmospheric Administration) to determine the warm and cold phases. Figure 5 shows the genesis density bias between El Niño and La Niña phases for both observations and model-simulated TCs using both the schemes. The changes in TC genesis frequency due to ENSO in observations (IBTrACS) show suppressed genesis during El Niño in the Bay of Bengal (Felton et al., 2013), increased genesis with a shift to the southeast region of the WNP (Wang & Chan, 2002; and Camargo et al., 2007), increased genesis with a shift toward the southwest in the ENP (Chia &

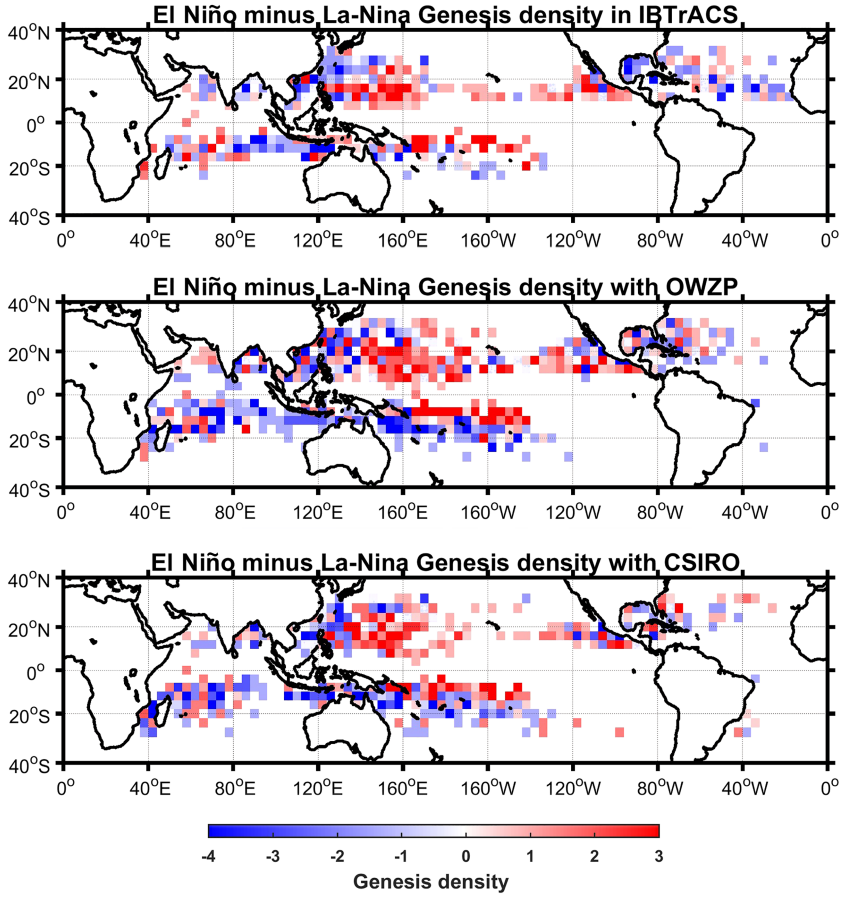

Figure 5. Geographical distribution of the difference in the TC genesis density of El Niño and La Niña years, with genesis density being the number of TCs per 4°×4° box region per year, for (top) IBTrACS, (center) ACCESS model with the OWZP detection scheme, and (bottom) ACCESS model with the CSIRO detection scheme.

Earth and Space Science

10.1029/2019EA000906

Table 3
Comparison of Tracking Schemes for Different TC Characteristics in the ACCESS Model and Reanalysis Data

Characteristics	OWZP (ERA-Interim)	CSIRO (ERA-Interim)	OWZP (Model)	CSIRO (model)	Remarks
Mean annual frequency	Similar to IBTrACS (75)	50% < IBTrACS (36.5)	50% > IBTrACS (143)	Similar to IBTrACS (86)	Better performance in ERA-Interim using the **OWZP scheme**
Spatial genesis density bias	(-ve) bias in the ENP, SP, and NA-MDR regions	(-ve) bias in almost all the ocean basins	(-ve) in the NA and AUS basins	Higher (-ve) bias in the NA-MDR; (-ve) bias in ENP, WNP, SI, and AUS basins	Better performance using the **OWZP** scheme in the model across the NA-MDR, ENP, and WNP
Mean genesis density bias	(-ve) bias in the ENP, SP, and NA-MDR regions	(-ve) bias in almost all the ocean basins	(-ve) bias in the NA-MDR region	Higher (-ve) bias in the SI, ENP, and NA-MDR region	Better performance of the **OWZP scheme** in the model across SI, ENP, and NA-MDR basins
Seasonal variability*	Similar to IBTrACS	Not captured in NI basin	Similar to IBTrACS	Not captured in NI basin	Captured the NI seasonal cycle by the **OWZP scheme**
Interannual variability*	Significant correlations in most of the ocean basins	Significant correlations in a few ocean basins	Significant correlations in only three ocean basins	Significant correlations in only two ocean basins	Performs better in the reanalysis compared to model using the **OWZP scheme**
Lifetime of storms	Similar to IBTrACS	Shorter than IBTrACS	Similar to IBTrACS	Shorter than IBTrACS	Better lifetime of tracks using the **OWZP** scheme in both reanalysis and the model
ENSO-induced changes in genesis locations	Similar to IBTrACS	Captured the ENSO changes in a few ocean basins	Captured signal in most of the ocean basins	Similar to the OWZP scheme except in NA and west coast of AUS	Better ENSO signal using the **OWZP** scheme in reanalysis and the model

Note. Bold text shows better performing detection scheme;
*indicates statistical correlations of mean TC frequency; -ve indicates negative.

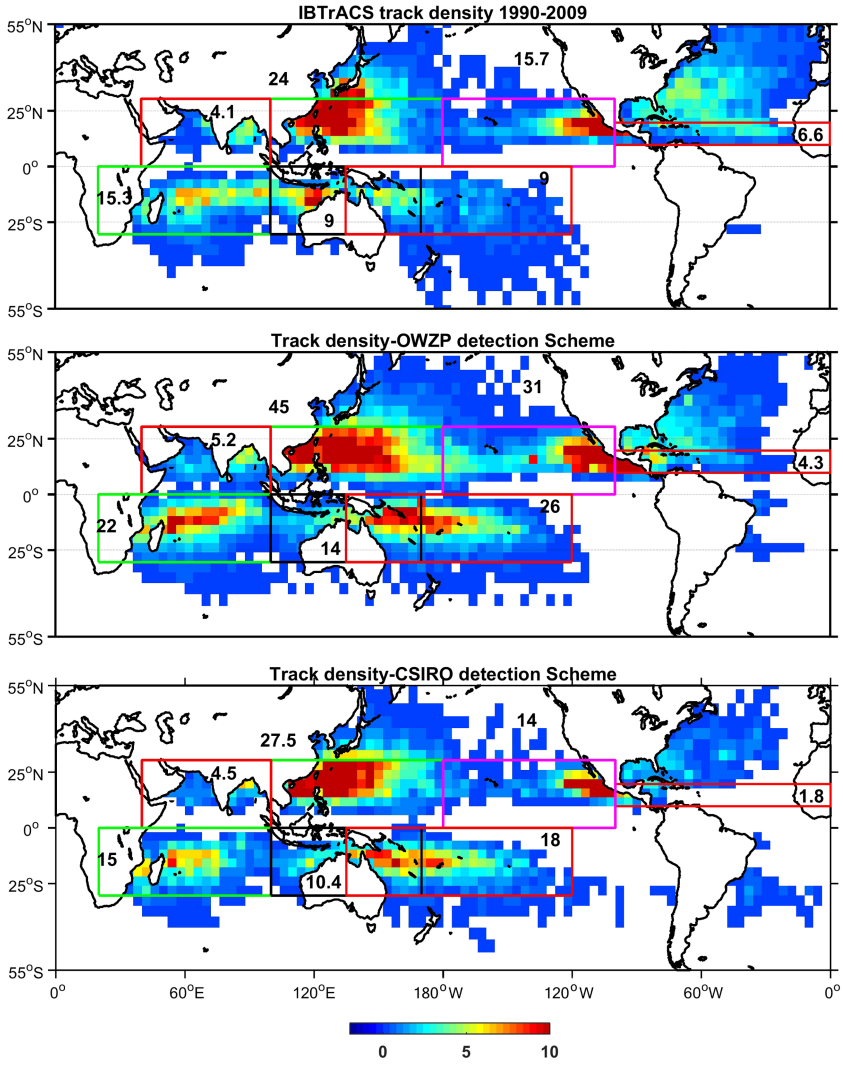

Figure 6. TC track density (the number of tracks per 4°×4° box region and per month) across the globe in both model and observations. The values in the box regions indicate the average annual storms in each ocean basin.

Ropelewski, 2002), and suppressed genesis in the NA basin due to increased VWS (Shaman et al., 2009). In the SH basins, there is increased genesis in the west of the SI Ocean (i.e., between 75°E and 135°E), suppressed genesis in the west of Australian basin (i.e., between 90°E and 135°E), and increased genesis in the SP close to the east coast of Australia (i.e., between 140°E and 170°E) (Kuleshov et al., 2008).

The model-simulated genesis frequency in the NH basins captures the increase and southeast shift in WNP, and increase and a southwest shift in ENP using both tracking schemes, and the suppressed TC genesis frequency in NA-MDR basin is captured to a lesser extent by the CSIRO detection scheme compared to the OWZP scheme. In the SH basins, the increased genesis in the SI Ocean (west of 135°E) and the east coast of Australia is captured moderately by both the schemes. Additionally, the suppressed genesis on the west coast of Australia basin is captured to a greater extent by the OWZP scheme compared to the CSIRO scheme. From the above analysis, we observe that both the tracking schemes can capture the major differences due to the ENSO phenomenon in most ocean basins. A similar analysis is performed in the reanalysis data with the OWZP scheme showing better performance compared to the CSIRO scheme (see Table 3 and Figure S6).

3.3. Geographical Distribution of Climatological TC Track Densities

The track density distribution is used to investigate the differences in the spatial distributions of TC tracks in the model using both the tracking algorithms. The tracks of each TC for the 20 years (i.e., 1990–2009)

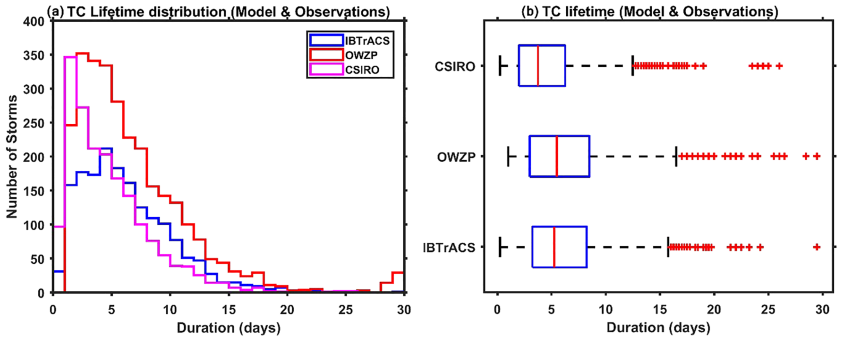

Figure 7. (a) Histograms of TC lifetime in both observations and model using both detection schemes. (b) Distributions of TC lifetime with the vertical line of the box indicate the median of the distribution, the left and right box edges are the 75th and 25th percentiles, the whiskers indicate the maximum and minimum values, and the red crosses indicate the outliers.

obtained from both the tracking schemes are composited per 4-degree box region and year across the globe, as shown in Figure 6. The OWZP scheme detected tracks have a wider spatial extent of track densities, indicating longer tracks and higher genesis frequency compared to the CSIRO detection scheme. The simulated track densities of both the schemes are well comparable with observations (IBTrACS) in most of the basins. The OWZP scheme better captures the track density across the Atlantic basin compared to the CSIRO scheme. In addition, the track density bias of Figure S7 shows strong negative bias in the north of the WNP basin using both the schemes and negative bias on the east coast of the ENP basin using the CSIRO detection scheme. Furthermore, the OWZP scheme has a more positive track bias in agreement with the positive bias in the genesis plots (Figure 3).

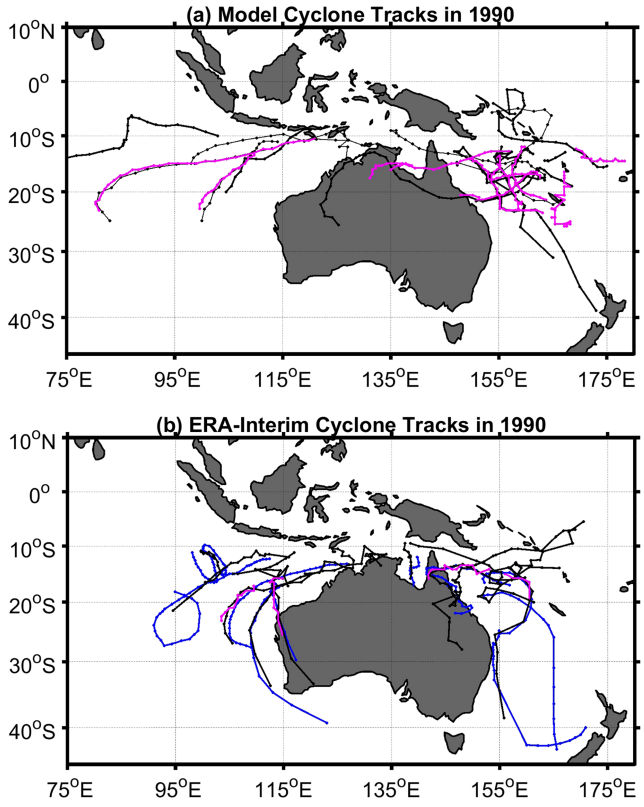

Figure 8. (a) TC tracks in ACCESS using both OWZP (black) and CSIRO (magenta) schemes. (b) TC tracks of the storms detected in the ERA-Interim using both CSIRO (magenta) and OWZP (black) detection schemes and IBTrACS (blue) for the year 1990.

Figure 7 shows the TC lifetime histograms of observations and storms detected in the model using both the schemes and their TC lifetime distributions. The CSIRO detected storms have shorter duration compared to the OWZP detected storms that have a longer duration almost similar to the observations. Similar results are observed in the reanalysis data with OWZP detected storms having longer lifetimes (Figure S8). These differences in the storm's lifetime may be partly due to differences in the duration thresholds, with 24 h in the CSIRO scheme and 48 h in the OWZP scheme. A recent study by Horn et al. (2014) also noted that TC lifetime is highly sensitive to the duration threshold of the tracking schemes.

3.4. Case Studies of TCs Detected by Both the Tracking Schemes Within the Model in the Australian Region

The CSIRO detected storms are found to be a subset of the OWZP detected storms in the ACCESS model data in all the basins, as shown in Figure S9. To understand the differences and similarities between the TCs detected using both the tracking schemes, the particular year 1990 is selected as a test case to see in detail the behavior of these storms. Figure 8a shows that CSIRO tracks are shorter and are a subset of OWZP tracks in the model, except one case of the CSIRO scheme, which has a different formation latitude and track compared to the OWZP scheme. A similar track analysis is performed using ERA-Interim reanalysis over the Australian region, and we observe that the CSIRO tracks are a subset of the OWZP detected tracks with lengthier tracks in the OWZP detected storms (Figure 8b). Also, the OWZP and the CSIRO detected tracks in the reanalysis closely resemble the IBTrACS tracks but are shorter. This may be partially due to an issue in IBTrACS rather than an inherent failing in the TC detection schemes. The lack of a consistent criterion for extratropical transition may be contributing to an artificial extension of IBTrACs well into the SH

midlatitudes (Sinclair, 2004). This can also be seen in Figure 6 south of New Zealand. The CSIRO scheme has fewer tracks across the basin aligned with fewer detections in the reanalysis. These results indicate that although both the tracking schemes are fundamentally different they show similarities in their storm tracks with longer tracks using the phenomenon-based tracking scheme (OWZP).

4. Discussion and Conclusion

In the current study, we examine differences between a phenomenon-based tracking scheme (OWZP) and a more traditional TC tracking scheme (CSIRO) in estimating the TC formation characteristics in the reanalysis and in a high-resolution ACCESS 1.3 climate model simulations run with interannually varying SSTs when compared against observations. A comparison of the sensitivity of TC formation to these two tracking schemes both in the model and reanalysis data is illustrated in Table 3. Although not many variations are observed in geographical TC distribution and interhemispheric asymmetry of global TC frequency, nevertheless noticeable differences can be observed in spatial TC genesis density bias regionally. The NA-MDR and the ENP regions in the model show a higher underestimation by the CSIRO scheme compared to the OWZP scheme (Table S3). The climatological biases in the large-scale climate variables of the model correspond to the biases of the genesis of both the tracking schemes (Sharmila et al., 2020). Different studies have noted that the climate models that simulate the TCs are sensitive to the convective parameterization schemes for producing deep convection (Camargo & Wing, 2016; Kim et al., 2012; Zhao et al., 2012). Therefore, either running the global models at high horizontal resolution (around 1 km) without the requirement of parameterization schemes or improving convection schemes may improve the model simulated large-scale variables that reduce the genesis biases.

Similarly, variations are observed in the global mean annual TC frequency of the model in both the schemes. Here the OWZP scheme shows higher frequency, while the CSIRO scheme is more comparable to the observations. The mean annual number in the reanalysis using the OWZP scheme is similar to observations, while the CSIRO scheme has fewer detections compared to observations. The increased TC numbers in the ACCESS model using the OWZP scheme may be due to grid resolution bias of the detection scheme but is smaller compared to the effect of the model physics, as stated by Tory, Chand, McBride, et al. (2013). Therefore, the increased number of detections using the OWZP detection scheme may be due to the more favorable large-scale climate of the ACCESS model. The reduced number of detections in the reanalysis using the CSIRO scheme is due to a resolution-dependent 10 m wind speed threshold, which causes an underestimation of TC numbers in the low-resolution reanalysis data sets (Hodges et al., 2017; Murakami, 2014). The resolution-dependent (CSIRO) TC tracking scheme has better performance in the high-resolution ACCESS model compared to the lower resolution reanalysis; we speculate that the model has improved the simulation of TC intensity compared with the reanalysis. ERA-Interim reanalyses are also not a perfect representation of TC characteristics, and the consistent underrepresentation of TC intensity in these reanalyses (e.g., Murakami, 2014) would lead to less reliable detection and (arguably) shorter TC tracks. Accordingly, a high-resolution model with improved model physics gives a better simulation of TC frequency and intensity characteristics, an improvement that is greater than merely the effect of less smoothing due to the improved model horizontal resolution (Walsh et al., 2013).

Also, the TC seasonal cycle of the model and reanalysis using both the tracking schemes has good statistical correlations when compared with observations in all the ocean basins except the NI Ocean, where the CSIRO tracking scheme has a weaker correlation due to higher TC detections in the monsoon season. In comparison, the OWZP scheme eliminates monsoon low detections in the NI Ocean. The model has statistically significant interannual correlations in the NA and ENP basins using the CSIRO scheme. In contrast, using the OWZP scheme, significant correlations are noted in the NA, WNP, and AUS basins (Table 2). The OWZP scheme has better interannual correlations in the reanalysis compared to the CSIRO scheme. The weaker interannual correlations in the model using the OWZP scheme compared to reanalysis may be due to the model's performance in simulating the large-scale fields and their temporal variation. It is also evident from the study that the CSIRO scheme detected storms are a subset of the OWZP detected storms, with shorter TC lifetime.

Although there are specific differences, the model's performance in simulating the geographical distribution, the relative percentage of TCs in each basin, seasonal variability (except NI), and ENSO-induced changes in

TC genesis locations using both schemes are comparable to the observations. From this analysis we see that the resolution-independent scheme has better performance in both the ACCESS model and the reanalysis. In contrast, the resolution-dependent scheme has better performance in simulating TC frequency characteristics in the ACCESS model compared to the reanalysis. Though model resolution plays a role in simulated TCs, it is not the only factor for better TC simulation in climate models. Therefore, this improved TC simulation in the high-resolution model using the CSIRO scheme may be due to increased horizontal resolution as well as improved model physics.

Future studies focus on applying this phenomenon based tracking scheme (OWZP) and resolution-dependent tracking scheme (CSIRO) to other current state-of-the-art high-resolution climate models. Comparisons across models are essential in climate projection studies as there exist differences in projections with different tracking schemes due to the fundamental differences between tracking schemes and also to threshold differences (Horn et al., 2014). Models with increased resolutions might reduce the differences between the tracking schemes as they better simulate the TC intensities. However, there are differences in detecting weaker storms with different schemes (Camargo & Wing, 2016). Therefore, there is a requirement for a tracking scheme that gives consistent results with different models at different resolutions. Also, applying these two schemes in idealized simulations (e.g., aqua-planet configurations) may improve our understanding of the large-scale climate controls on TC formation, as well as better understanding the influence of detection schemes on these relationships.

Acknowledgments
We are grateful to the Melbourne India Postgraduate Program for providing the first author with funding to carry out her PhD at the University of Melbourne. We also thank the Australian Research Council Centre of Excellence for Climate Extremes (grant CE170100023) and the Earth Systems and Climate Change Hub of the National Environmental Science Program for providing partial funding. We want to thank the ACCESS modeling group and the National Computational Infrastructure system, supported by the Australian government, for providing the model and computing time and space on the supercomputer (Raijin). The preprocessed model and reanalysis data are available at the following link: https://doi.org/10.26188/5e26eb56a17d2.

References

Bell, R., Strachan, J., Vidale, P. J., Hodges, K., & Roberts, M. (2013). Response of tropical cyclones to idealized climate change experiments in a global high-resolution coupled general circulation model. *J. Clim.*, *26*, 7966–7980.

Bell, S. S., Chand, S. S., Tory, K. J., Dowdy, A. J., Turville, C., & Ye, H. (2019). Projections of Southern Hemisphere tropical cyclone track density using CMIP5 models. *Climate Dyn.*, *52*, 6065–6079.

Bell, S. S., Chand, S. S., Tory, K. J., & Turville, C. (2018). Statistical assessment of the OWZ tropical cyclone tracking scheme in ERA-Interim. *J. Clim.*, *31*, 2217–2232.

Bell, S. S., Chand, S. S., Tory, K. J., Turville, C., & Ye, H. (2019). Eastern North Pacific tropical cyclone activity in historical and future CMIP5 experiments: Assessment with a model-independent tracking scheme. *Climate Dyn.*, *53*, 4841–4855.

Bengtsson, L., Hodges, K. I., & Esch, M. (2007). Tropical cyclones in a T159 resolution global climate model: Comparison with observations and re-analyses. *Tellus A: Dynam. Meteorol. Oceanogr.*, *59*, 396–416.

Bengtsson, L., Hodges, K. I., Esch, M., Keenlyside, N., Kornblueh, L., Luo, J. J., & Yamagata, T. (2007). How may tropical cyclones change in a warmer climate? *Tellus A: Dynam. Meteorol. Oceanogr.*, *59*, 539–561.

Best, M.J., M. Pryor, D.B. Clark, G. G Rooney, R. Essery, C.B. Ménard, J.M. Edwards, et al. (2011), The Joint UK Land Environment Simulator (JULES), model description–Part 1: Energy and water fluxes. *Geosci. Model Dev.*, *4*, 677-699.

Bi, D., Dix, M., Marsland, S. J., O'Farrell, S., Rashid, H., Uotila, P., et al. (2013). The ACCESS coupled model: Description, control climate and evaluation. *Aust. Meteorol. Oceanogr. J*, *63*, 41–64.

Bister, M., & Emanuel, K. A. (1997). The genesis of Hurricane Guillermo: TEXMEX analyses and a modeling study. *Mon. Weather Rev.*, *125*, 2662–2682.

Brown, A. R., Beare, R. J., Edwards, J. M., Lock, A. P., Keogh, S. J., Milton, S. F., & Walters, D. N. (2008). Upgrades to the boundary-layer scheme in the Met Office numerical weather prediction model. *Bound.-Lay. Meteorol.*, *128*, 117–132.

Camargo, S., Sobel, A., Barnston, A., & Klotzbach, P. (2010). The influence of natural climate variability, and seasonal forecasts of tropical cyclone activity. In J. C. L. Chan, & J. D. Kepert (Eds.), *Global Perspectives on Tropical Cyclones*, (2nd ed.pp. 325–360). Singapore: World Scientific Publishing Co.

Camargo, S. J., Barnston, A. G., Klotzbach, P. J., & Landsea, C. W. (2007). Seasonal tropical cyclone forecasts. *WMO Bull.*, *56*, 297.

Camargo, S. J., Barnston, A. G., & Zebiak, S. E. (2005). A statistical assessment of tropical cyclones in atmospheric general circulation models. *Tellus*, *57*, 589–604.

Camargo, S. J., Sobel, A. H., Delgenio, A. D., Jonas, J. A., Kelley, M., Lu, Y., et al. (2016). Tropical cyclones in the GISS ModelE2. *Tellus A: Dyn. Meteorol. Oceanogr.*, *68*, 31494.

Camargo, S. J., & Wing, A. A. (2016). Tropical cyclones in climate models. *Wil. Inter. Rev.: Climate Change*, *7*, 211–237.

Chia, H. H., & Ropelewski, C. F. (2002). The interannual variability in the genesis location of tropical cyclones in the northwest Pacific. *J. Clim.*, *15*, 2934–2944.

Compo, G. P., Whitaker, J. S., Sardeshmukh, P. D., Matsui, N., Allan, R. J., Yin, X., et al. (2011). The twentieth century reanalysis project. *Q. J. Roy. Meteorol. Soc.*, *137*, 1–28.

Davis, C. A., & Ahijevych, D. A. (2012). Mesoscale structural evolution of three tropical weather systems observed during PREDICT. *J. Atmos. Sci.*, *69*, 1284–1305.

Dee, D. P., Uppala, S. M., Simmons, A. J., Berrisford, P., Poli, P., Kobayashi, S., et al. (2011). The ERA-Interim reanalysis: Configuration and performance of the data assimilation system. *Q. J. Roy. Meteorol. Soc.*, *137*, 553–597.

Dunkerton, T. J., Montgomery, M. T., & Wang, Z. (2009). Tropical cyclogenesis in a tropical wave critical layer: Easterly waves. *Atmos. Chem. Phys.*, *9*.

Edwards, J. M., & Slingo, A. (1996). Studies with a flexible new radiation code. I: Choosing a configuration for a large-scale model. *Q. J. Roy. Meteorol. Soc.*, *122*, 689–719.

Emanuel, K. (2003). Tropical cyclones. *Annu. Rev. Earth Planet. Sci.*, *31*, 75–104.

Felton, C. S., Subrahmanyam, B., & Murty, V. S. N. (2013). ENSO-modulated cyclogenesis over the Bay of Bengal. *J. Clim.*, *26*, 9806–9818.

Gray, W. M. (1968). Global view of the origin of tropical disturbances and storms. *Mon. Weather Rev.*, *110*, 572–586.

Gray, W. M. (1975). Tropical cyclone genesis. Dept. of Atmos. Sci. Paper No. 232, Colorado State University, Ft. Collins, CO, 121.
Hendricks, E. A., Montgomery, M. T., & Davis, C. A. (2004). The role of "vortical" hot towers inthe formation of tropical cyclone Diana (1984). *Journal of the Atmospheric Sciences*, *61*, 1209–1232.
Hodges, K., Cobb, A., & Vidale, P. L. (2017). How well are tropical cyclones represented in reanalysis datasets? *J. Clim.*, *30*, 5243–5264.
Hodges, K. I., & Emerton, R. (2015). The prediction of Northern Hemisphere tropical cyclone extended life cycles by the ECMWF ensemble and deterministic prediction systems. Part I: Tropical cyclone stage. *Mon. Wea. Rev.*, *143*, 5091–5114.
Horn, M., Walsh, K., Zhao, M., Camargo, S. J., Scoccimarro, E., Murakami, H., et al. (2014). Tracking scheme dependence of simulated tropical cyclone response to idealized climate simulations. *J. Clim.*, *27*, 9197–9213.
Kanamitsu, M., Ebisuzaki, W., Woollen, J., Yang, S. K., Hnilo, J. J., Fiorino, M., & Potter, G. L. (2002). NCEP–DOE AMIP-II reanalysis (r-2). *Bull. Am. Meteorol. Soc.*, *83*, 1631–1644.
Kim, D., Sobel, A. H., Del Genio, A. D., Chen, Y., Camargo, S. J., Yao, M. S., et al. (2012). The tropical subseasonal variability simulated in the NASA GISS general circulation model. *J. Clim.*, *25*, 4641–4659.
Knapp, K. R., Kruk, M. C., Levinson, D. H., Diamond, H. J., & Neumann, C. J. (2010). The international best track archive for climate stewardship (IBTrACS) unifying tropical cyclone data. *Bull. Amer. Meteor. Soc.*, *91*, 363–376.
Knutson, T., McBride, J. L., Chan, J., Emanuel, K., Holland, G., Landsea, C., et al. (2010). Tropical cyclones and climate change. *Nature Geoscience*, *3*, 157.
Kuleshov, Y., Qi, L., Fawcett, R., & Jones, D. (2008). On tropical cyclone activity in the Southern Hemisphere: Trends and the ENSO connection. *Geophys. Res. Lett.*, *35*(14), L14S08. https://doi.org/10.1029/2007GL032983
Li, H., & Sriver, R. L. (2018). Tropical cyclone activity in the high-resolution Community Earth System Model and the impact of ocean coupling. *J. Adv. Model. Earth Syst.*, *10*, 165–186.
Lock, A. P. (2001). The numerical representation of entrainment in parameterizations of boundary layer turbulent mixing. *Mon. Weather Rev.*, *129*, 1148–1163.
Lock, A. P., Brown, A. R., Bush, M. R., Martin, G. M., & Smith, R. N. B. (2000). A new boundary layer mixing scheme. Part I: Scheme description and single-column model tests. *Mon. Weather Rev.*, *128*, 3187–3199.
Manganello, J. V., Hodges, K. I., Kinter, J. L. III, Cash, B. A., Marx, L., Jung, T., et al. (2012). Tropical cyclone climatology in a 10-km global atmospheric GCM: Toward weather-resolving climate modeling. *J. Clim.*, *25*, 3867–3893.
McBride, J. L., & Zehr, R. (1981). Observational analysis of tropical cyclone formation. Part II: Comparison of non-developing versus developing systems. *J. Atmos. Sci.*, *38*, 1132–1151.
Montgomery, M. T., Davis, C., Dunkerton, T., Wang, Z., Velden, C., Torn, R., et al. (2012). The Pre-Depression Investigation of Cloud-Systems in the Tropics (PREDICT) experiment: Scientific basis, new analysis tools, and some first results. *Bull. Am. Meteorol. Soc.*, *93*, 153–172.
Montgomery, M. T., Lussier, L. L. III, Moore, R. W., & Wang, Z. (2010). The genesis of Typhoon Nuri as observed during the tropical cyclone structure 2008 (TCS-08) field experiment—Part 1: The role of the easterly wave critical layer. *Atmos. Chem. Phys.*, *10*, 9879–9900.
Murakami, H. (2014). Tropical cyclones in reanalysis data sets. *Geophys. Res. Lett.*, *41*, 2133–2141.
Murakami, H., Mizuta, R., & Shindo, E. (2012). Future changes in tropical cyclone activity projected by multi-physics and multi-SST ensemble experiments using the 60-km-mesh MRI-AGCM. *Clim. Dyn.*, *39*, 2569–2584.
Murakami, H., Sugi, M., & Kitoh, A. (2013). Future changes in tropical cyclone activity in the North Indian Ocean projected by high-resolution MRI-AGCMs. *Clim. Dyn.*, *40*, 1949–1968.
Murakami, H., Wang, B., & Kitoh, A. (2011). Future change of western North Pacific typhoons: Projections by a 20-km-mesh global atmospheric model. *J. Clim.*, *24*, 1154–1169.
Oouchi, K., Yoshimura, J., Yoshimura, H., Mizuta, R., Kusunoki, S., & Noda, A. (2006). Tropical cyclone climatology in a global-warming climate as simulated in a 20 km-mesh global atmospheric model: Frequency and wind intensity analyses. *J. Meteorol. Soc. Jap. Ser. II*, *84*, 259–276.
Ren, F., Liang, J., Wu, G., Dong, W., & Yang, X. (2011). Reliability analysis of climate change of tropical cyclone activity over the western North Pacific. *J. Climate*, *24*, 5887–5898.
Riemer, M., Montgomery, M. T., & Nicholls, M. E. (2010). A new paradigm for intensity modification of tropical cyclones: Thermodynamic impact of vertical wind shear on the inflow layer. *Atmos. Chem. Phys.*, *10*(7), 3163–3188. https://doi.org/10.5194/acp-10-3163-2010
Schreck, C. J. III, Knapp, K. R., & Kossin, J. P. (2014). The impact of best track discrepancies on global tropical cyclone climatologies using IBTrACS. *Mon. Wea. Rev.*, *142*, 3881–3899.
Shaevitz, D. A., Camargo, S. J., Sobel, A. H., Jonas, J. A., Kim, D., Kumar, A., et al. (2014). Characteristics of tropical cyclones in high-resolution models in the present climate. *J. Adv. Model. Earth Syst.*, *6*, 1154–1172.
Shaman, J., Esbensen, S. K., & Maloney, E. D. (2009). The dynamics of the ENSO–Atlantic hurricane teleconnection: ENSO-related changes to the North African–Asian jet affect Atlantic basin tropical cyclogenesis. *J. Clim.*, *22*, 2458–2482.
Sharmila, S., & Walsh, K. J. E. (2017). Impact of large-scale dynamic versus thermodynamic climate conditions on contrasting tropical cyclone genesis frequency. *J. Clim.*, *30*, 8865–8883.
Sharmila, S., Walsh, K. J. E., Thatcher, M., Wales, S., & Utembe, S. (2020). Real world and tropical cyclone world. Part I: High-resolution climate model verification. *J. Clim.*, *33*, 1455–1472.
Sinclair, M. R. (2004). Extratropical transition of southwest Pacific tropical cyclones. Part II: Midlatitude circulation characteristics. *Mon. Wea. Rev*, *132*, 2145–2168.
Strachan, J., Vidale, P. L., Hodges, K., Roberts, M., & Demory, M. E. (2013). Investigating global tropical cyclone activity with a hierarchy of AGCMs: The role of model resolution. *J. Clim.*, *26*, 133–152.
Tang, B., & Emanuel, K. (2010). Midlevel ventilation's constraint on tropical cyclone intensity. *J. Atmos. Sci.*, *67*(6), 1817–1830.
Tory, K. J., Chand, S. S., Dare, R. A., & McBride, J. L. (2013a). The development and assessment of a model-, grid-, and basin-independent tropical cyclone detection scheme. *J. Clim.*, *26*, 5493–5507.
Tory, K. J., Chand, S. S., Dare, R. A., & McBride, J. L. (2013b). An assessment of a model-, grid-, and basin-independent tropical cyclone detection scheme in selected CMIP3 global climate models. *J. Clim.*, *26*, 5508–5522.
Tory, K. J., Chand, S. S., McBride, J. L., Ye, H., & Dare, R. A. (2013). Projected changes in late-twenty-first-century tropical cyclone frequency in 13 coupled climate models from phase 5 of the Coupled Model Intercomparison Project. *J. Clim.*, *26*, 9946–9959.
Tory, K. J., Dare, R. A., Davidson, N. E., McBride, J. L., & Chand, S. S. (2013). The importance of low-deformation vorticity in tropical cyclone formation. *Atmos. Chem. Phys.*, *13*, 2115–2132.
Vecchi, G. A., & Soden, B. J. (2007). Effect of remote sea surface temperature change on tropical cyclone potential intensity. *Nature*, *450*, 1066–1070.

Vitart, F., Anderson, J. L., & Stern, W. F. (1997). Simulation of interannual variability of tropical storm frequency in an ensemble of GCM integrations. *J. Clim.*, *10*, 745–760.
Vitart, F., Anderson, J. L., & Stern, W. F. (1999). Impact of large-scale circulation on tropical storm frequency, intensity, and location, simulated by an ensemble of GCM integrations. *J. Clim.*, *12*, 3237–3254.
Walsh, K., Lavender, S., Scoccimarro, E., & Murakami, H. (2013). Resolution dependence of tropical cyclone formation in CMIP3 and finer resolution models. *Clim. Dyn.*, *40*, 585–599.
Walsh, K. J., Camargo, S. J., Vecchi, G. A., Daloz, A. S., Elsner, J., Emanuel, K., et al. (2015). Hurricanes and climate: The US CLIVAR working group on hurricanes. *Bull. Am. Meteorol. Soc.*, *96*, 997–1017.
Walsh, K. J., McBride, J. L., Klotzbach, P. J., Balachandran, S., Camargo, S. J., Holland, G., et al. (2016). Tropical cyclones and climate change. *Wil. Inter. Rev.: Climate Change*, *7*, 65–89.
Walsh, K. J. E., Fiorino, M., Landsea, C. W., & McInnes, K. L. (2007). Objectively determined resolution-dependent threshold criteria for the detection of tropical cyclones in climate models and reanalysis. *J. Clim.*, *20*, 2307–2314.
Walters, D., Brooks, M., Boutle, I., Melvin, T., Stratton, R., Vosper, S., et al. (2017). The Met Office unified model global atmosphere 6.0/6.1 and JULES global land 6.0/6.1 configurations. *Geosci. Model Dev.*, *10*, 1487–1520.
Wang, B., & Chan, J. C. (2002). How strong ENSO events affect tropical storm activity over the western North Pacific. *J. Clim.*, *15*, 1643–1658.
Wang, Z. (2012). Thermodynamic aspects of tropical cyclone formation. *J. Atmos. Sci.*, *69*, 2433–2451.
Wang, Z., Montgomery, M. T., & Dunkerton, T. J. (2009). A dynamically-based method for forecasting tropical cyclogenesis location in the Atlantic sector using global model products. *Geophys. Res. Lett.*, *36*.
Wang, Z., Montgomery, M. T., & Dunkerton, T. J. (2010a). Genesis of pre–Hurricane Felix (2007a). Part I: The role of the easterly wave critical layer. *J. Atmos. Sci.*, *67*, 1711–1729.
Wang, Z., Montgomery, M. T., & Dunkerton, T. J. (2010b). Genesis of pre–Hurricane Felix (2007b). Part II: Warm core formation, precipitation evolution, and predictability. *J. Atmos. Sci.*, *67*, 1730–1744.
Wilson, D. R., Bushell, A. C., Kerr-Munslow, A. M., Price, J. D., & Morcrette, C. J. (2008). PC2: A prognostic cloud fraction and condensation scheme. I: Scheme description. *Q. J. Roy. Meteorol. Soc.*, *134*, 2093–2107.
Zhao, M., Held, I. M., & Lin, S. J. (2012). Some counterintuitive dependencies of tropical cyclone frequency on parameters in a GCM. *J. Atmos. Sci.*, *69*, 2272–2283.
Zhao, M., Held, I. M., Lin, S. J., & Vecchi, G. A. (2009). Simulations of global hurricane climatology, interannual variability, and response to global warming using a 50-km resolution GCM. *J. Clim.*, *22*, 6653–6678.